IEEE Access
Multidisciplinary ⋮ Rapid Review ⋮ Open Access Journal

Received January 19, 2021, accepted February 5, 2021, date of publication February 9, 2021, date of current version February 18, 2021.

Digital Object Identifier 10.1109/ACCESS.2021.3058120

Four-Directional Total Variation With Overlapping Group Sparsity for Image Denosing

XIANCHUN ZHOU[1,2] AND MENGJIA FAN[1]

[1]College of Electronic and Information Engineering, Nanjing University of Information Science and Technology, Nanjing 210044, China
[2]Jiangsu Collaborative Innovation Center of Atmospheric Environment and Equipment Technology, Nanjing University of Information Science and Technology, Nanjing 210044, China

Corresponding author: Xianchun Zhou (001398@nuist.edu.cn)

This work was supported in part by National Natural Science Foundation of China under Grant 11202106, and in part by National Natural Science Foundation of China under Grant 61302188.

ABSTRACT In this paper, a new model combining four-directional total variation with overlapping group sparsity is proposed, which not only suppresses the staircase effects introduced by traditional total variation, but also fully utilizes the gradient neighborhood information on each pixel of the image. In order to decrease the computation time of image denoising, the alternating direction method of multipliers (ADMM) is adopted to divide the complex optimization problem into separate subproblems that are easy to solve. At the same time, two-dimensional Fast Fourier Transform (FFT) and majorization-minimization (MM) are used to solve the subproblems alternatively. Then, the proposed new model is compared with other state-of-the-art models. Experiments show that the new model is robust in denoising. The new model not only excavates the gradient information of the four directions on the image to remove the noise more effectively, but also better in preserving image features, further reducing staircase artifacts.

INDEX TERMS Image denoising, four-directional total variation, overlapping group sparsity, ADMM.

I. INTRODUCTION

Due to the imperfection of an imaging system, images tend to be corrupted by different levels of noise during the progress of image capture, transmission, and storage, which can reduce image quality and cause image degradation. Therefore, image restoration as one of the processing technologies is significant in image processing.

Image restoration is a classical ill-posed inverse problem [1]. The main purpose of image restoration is to obtain an estimate of the original image from the degraded image. There are many restoration methods to solve the ill-posed inverse image problem. He *et al.* [2] presented a deep residual learning framework to address the image degradation problem. Zhang *et al.* [3] proposed a deep convolutional neural network denoising model (DnCNN) based on residual learning and batch normalization. The denoising effect of DnCNN model is remarkable, but the training time is long due to its full convolution network structure. Zhang *et al.* [4] also proposed a new fast and flexible denoising convolutional neural network model (FFDNet) with the use of noise level maps as input. It can effectively deal with the noise of more complex real scenes. Lysaker and Tai [5] combined total variation filter with a fourth-order partial differential equation (PDE) filter. This method achieves a good trade-off between preserving edges and suppressing the staircase effect. Zhou *et al.* [6] presented an image denoising model with dual driving forces of gradient and curvature, which significantly improved the image clarity. A denoising model based on block matching and 3D filtering (BM3D) is introduced in [7]. It achieves good performance in image denoising.

Since most of the noise is random, the image signal has obvious sparse characteristics in some transform domain or gradient domain. The key to tackle the ill-posed problem is regularization, that is, some prior information about the original image is integrated into the solution of the inverse image problem, so as to suppress noise and obtain a smooth (regular) solution. Rudin *et al.* [8] introduced a total variation (TV) model for image restoration, which is a typical regularization method and widely used. This model has the ability to preserve image features (edge, texture pattern), but it also produces some unwanted staircase artifacts cause it assumes the image as piece-wise smooth.

Based on that, many extended models of TV were proposed to reduce the staircase artifacts. Hu *et al.* [9] proposed a generalized higher degree total variation regularization (HDTV), which utilizes high-order derivatives in all directions of the image to build a model to solve the optimization

The associate editor coordinating the review of this manuscript and approving it for publication was Naveed Akhtar.

problem. The total generalized variation (TGV) proposed by Bredies *et al.* [10] can suppress the staircase effects by balancing the first and second derivative regularizations. Liu *et al.* [11] proposed a generalized total variation-based MRI denoising model, this model can reduce the noise present in magnitude MR images effectively. Xu *et al.* [12] applied the curvature term to removing multiplicative noise and preserving smoothness. The nonlocal total variation model (NLTV) [13] is a popular and effective denoising model using the nonlocal gradient of the image as the regularization term. Liu *et al.* [14] successfully applied the NLTV model to Magnetic resonance image denoising.

A model composed of total variation and high-order total variation is proposed in [15]. This hybrid model utilizes total variation regularization term to preserve edges and utilizes high-order total variation to reduce staircase artifacts. Although using higher-order total variation instead of traditional total variation can alleviate staircase effects more effectively, it will over smooth image edge for sharp image. Chan *et al.* [16] added a box constraint to the TV model (TV+BOX), so that the restored image could get a clearer image with a certain interval. Chen *et al.* [17] used the split Bregman iterative algorithm to solve the anisotropic TV so as to reduce the computation time and have good restoration with sharp edges.

Liu *et al.* [18] considered the total variation with overlapping group sparsity (OGSTV) for image restoration under Gaussian noise. This method extends the gradient of pixel level to the overlapping group sparse gradient in order to promote the difference between the smooth region and edge region and better suppress staircase effects. Shi *et al.* [19] adopted hyper-Laplacian prior with overlapping group sparsity for image restoration. The new model achieves a good balance between preserving features and overcoming staircase effects. Adam *et al.* [20] combined non-convex higher order TV with overlapping group sparsity to construct a hybrid model (HNHOTV), so that it can maintain the uniformity of the staircase edge. Kumar *et al.* [21] proposed a model of combing higher order fractional TV and overlapping group sparsity to retain the texture pattern in the image while decrease staircase artifacts. In our previous work [22], we combined high-order total variation with overlapping group sparsity (OGSHOTV). The mixture model could better suppress the staircase effect and preserve the details in image edges. Recently, overlapping group sparsity has been applied to figure out Cauchy noise [23], Poisson noise [24], and speckle noise [25], demonstrating its effectiveness.

The methods mentioned above merely contain gradient information in the vertical and horizontal directions, but ignores gradient in the diagonal and back-diagonal directions. Four-directional total variation (TV4) [26] can make full use of the neighbor gradient information of each pixel. A new four-directional total variation model proposed by Liao *et al.* [27] takes gradient information in the diagonal and back-diagonal directions into account. They solved the optimization problem with gradient projection (GP) and also given a complete mathematical proof for the first time. However, the efficiency of GP depends on the update rate. When the update rate is too large, the gradient projection algorithm does not converge; when the update rate is too small, the operation efficiency is low. Wu *et al.* [28] proposed to group fractional order total variation and four directions total variation into a hybrid model. To reduce the computation time, they used split Bregman algorithm and fast Fourier transform (FFT) to solve the problem. Cheng *et al.* [29] assumed that the degraded image satisfies the periodic boundary condition, then they adopted FFT and alternating direction method of multipliers (ADMM) to solve TV4 model. This model reduces the calculation time greatly while relieves staircase effects.

Based on prior researches, we propose a new hybrid model called four-directional total variation with overlapping group sparsity (OGSTV4) by taking advantage of TV4 and OGSTV denoising model. The main contributions of this paper are as follows:

(1) the new model combines gradient information of each pixel in four directions (vertical, horizontal, diagonal and back-diagonal) to form a new sparse regularize constraint, that is, non-separated group gradient.
(2) To reduce computation time of image restoration, we use ADMM algorithm to divide the constrained optimization problem into separate subproblems by introducing split variables and dual variables.
(3) Assuming that image satisfies periodic boundary conditions and the difference matrices operation in four directions of the image is regarded as convolution operation, we employ FFT [30], [31] and majorization-minimization (MM) [32], [33] to solve the subproblem alternatively.

The rest of this paper is organized as follows. In the next section, four-direction total variation, overlapping group sparse regularization and ADMM algorithm are briefly described. In Sec.III, The new model proposed in this paper is introduced in detail. In Sec.IV, we adjust the parameters and compare with other state-of-art models to demonstrate the effectiveness of the new model. Conclusions are presented in Sec.V.

II. RELATED WORK

A. FOUR-DIRECTIONAL TOTAL VARIATION

The image degradation process can be modeled with the following linear system:

$$f = Hu + \eta \tag{1}$$

where $u \in R^{mn\times 1}$ is the original image, $f \in R^{mn\times 1}$ represents the blurred and noisy degraded image, $H \in R^{mn\times mn}$ is a linear operator constructed by the discrete point spread function (PSF), e.g., convolution operator, identity operator, etc. In this paper, H is an identity operator, that is, $H = I$, which constitutes the denoising problem. $\eta \in R^{mn\times 1}$ is additive Gaussian white noise. Then the traditional TV model is as

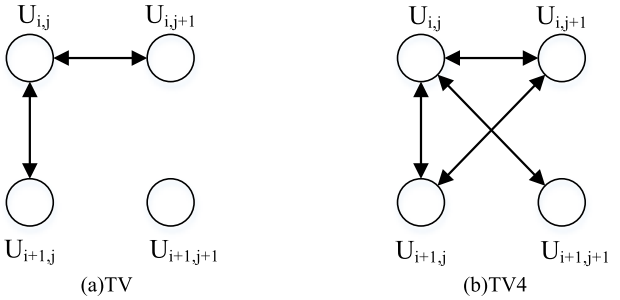

FIGURE 1. Comparison of the gradient information in TV and TV4.

follows:

$$\hat{u} = \min_{u} \frac{1}{2} \|f - Hu\|_2^2 + \mu \varphi_{TV}(u) \tag{2}$$

where $\|\cdot\|_2$ is the Euclidean norm and $\hat{u}$ is the optimal solution. The first term in the equation (2) is the data fidelity term, which keeps the original data u close enough to the input data f. The second term $\varphi_{TV}(u)$ is the regularization function, which is used to control noise and artifacts in data and simulate the prior knowledge of unknown data. $\mu > 0$ is the regularization parameter that balances the two terms. Typical anisotropic total variation is defined as:

$$\varphi_{TV}(u) = \|D_h u\|_1 + \|D_v u\|_1 \tag{3}$$

where $D_h \in R^{mn \times mn}$ and $D_v \in R^{mn \times mn}$ are respectively difference matrices along horizontal and vertical directions, $\|\bullet\|_1$ represents the norm of matrix L1.

It can be seen that typical TV model only considers the gradient information in vertical and horizontal directions refer to (3). The probability of a pixel being polluted by noise is much higher than that of four surrounding points being polluted by noise at the same time. To reduce noise more comprehensively, Sakurai *et al.* proposed a four-directional total variation model [26], which takes the image gradients in diagonal and back-diagonal directions into account to fully utilize the neighbor gradient information of each pixel. Figure 1 is a comparison of the gradient information in TV and TV4.

From Figs.1, we see that TV4 can suppress more noise in four directions, further improving the quality of image restoration. The regularization term of four-directional total variation model is defined as:

$$\varphi_{TV4}(u) = \|D_h u\|_1 + \|D_v u\|_1 + \|D_d u\|_1 + \|D_b u\|_1 \tag{4}$$

where $D_d \in R^{mn \times mn}$ and $D_v \in R^{mn \times mn}$ represent the difference matrices in the diagonal and back-diagonal direction, respectively.

B. OVERLAPPING GROUP SPARSITY PRIOR

Liu and Selesnick *et al.* defined a K-point group of the vector $x \in R^n$[34]by

$$x_{i,K} = [x(i), \cdots, x(i+K-1)] \in R^K \tag{5}$$

$x_{i,K}$ can be regarded as a block of K contiguous samples of a starting at index i. For one dimensional case, overlapping group sparsity regularization term is shown as:

$$\varphi(x) = \sum_{i=1}^{n} \|x_{i,K}\|_2 \tag{6}$$

where K determines the group size. For two dimensional case, a $K \times K$ point group of the image $v \in R^{n \times n}$ is defined as:

$$\tilde{v}_{i,j,K,K} = \begin{bmatrix} v_{i-a_1,j-a_1} & v_{i-a_1,j-a_1+1} & \cdots & v_{i-a_1,j+a_2} \\ v_{i-a_1+1,j-a_1} & v_{i-a_1+1,j-a_1+1} & \cdots & v_{i-a_1,+1,j+a_2} \\ \vdots & \vdots & \ddots & \\ v_{i+a_1,j-a_1} & v_{i+a_1,j-a_1+1} & \cdots & v_{i+a_2,j+a_2} \end{bmatrix} \in R^{K \times K} \tag{7}$$

where $a_1 = \left\lfloor \frac{K-1}{2} \right\rfloor, a_2 = \left\lfloor \frac{K}{2} \right\rfloor$, and $\lfloor x \rfloor$ represents the greatest integer less than or equal to x. Let $v_{i,j,K,K}$ be a vector obtained by arranging all elements of $\tilde{v}_{i,j,K,K}$ in lexicographic order. The overlapping group sparsity regularization term of the two-dimensional array is shown as:

$$\varphi(v) = \sum_{i=1}^{n} \sum_{j=i}^{n} \|v_{i,j,K,K}\|_2 \tag{8}$$

In particular, $\varphi(v)$ is the anisotropic total variation function when $K = 1$.

C. ADMM

Alternative direction method of multipliers (ADMM) is a computational framework for solving optimization problems[31], which is suitable for solving distributed convex optimization problems. ADMM decomposes the large global problem into several smaller local sub-problems which can be easily solved, and obtains the optimal solution through decomposition coordination. The algorithm generally solves the following optimization problems:

$$\begin{aligned} &\min_{x_1, x_2} f(x_1) + g(x_2) \\ &s.t.\ \mathbf{A}x_1 + \mathbf{B}x_2 = c \\ &\quad x_i \in \chi_i, i = 1, 2 \end{aligned} \tag{9}$$

where $\chi_i \in R^{m_i}$ are the nonempty closed convex set, $\mathbf{A}, \mathbf{B} \in R^{i \times m_i}$ are Linear transformation matrices, $f(\cdot), g(\cdot) : \chi \to \mathrm{R}$ are closed convex function, and $c \in R^l$ is a given vector. With the Lagrangian multiplier $p \in R^l$ to the linear constraint stated in problem (8), the augmented Lagrangian function is followed as:

$$\begin{aligned} L_A(x_1, x_2, p) = &f(x_1) + g(x_2) + p^T(\mathbf{A}x_1 + \mathbf{B}x_2 - c) \\ &+ \frac{\delta}{2} \|\mathbf{A}x_1 + \mathbf{B}x_2 - c\|_2^2 \end{aligned} \tag{10}$$

where $\delta > 0$ is the penalty parameter.

According to the framework of ADMM, the goal is to find the saddle point in problem (9) by alternatively minimizing

scheme. Then we obtain the following ADMM iterative minimization problem:

Algorithm1.ADMM for the minimization problem (9)

1: Initialize $x_1^0, x_2^0, \mathrm{p}^0, \delta > 0$

2: For $k = 1, 2, \cdots$, compute $x_1^{k+1}, x_2^{k+1}, p^{k+1}$

$$x_1^{k+1} = \arg\min_{x_1} f(x_1) + \frac{\delta}{2}\left\|\mathbf{A}x_1 + \mathbf{B}x_2^k - c + \frac{p^k}{\delta}\right\|_2^2$$

$$x_2^{k+1} = \arg\min_{x_2} g(x_1) + \frac{\delta}{2}\left\|\mathbf{A}x_1^{k+1} + \mathbf{B}x_2 - c + \frac{p^k}{\delta}\right\|_2^2$$

$$p^{k+1} = p^k + \delta(\mathbf{A}x_1^{k+1} + \mathbf{B}x_2^{k+1} - c)$$

$$k = k + 1$$

3: Until a stopping criterion is satisfied

III. PROPOSED MODEL

In this section, a novel model coupling with **overlapping group sparsity and four-directional total variation is defined as:**

$$\hat{f} = \arg\min_u \frac{1}{2}\|f-u\|_2^2 + \mu\varphi\left(\|D_h u\|_1 + \|D_v u\|_1 + \|D_d u\|_1 + \|D_b u\|_1\right) \tag{11}$$

where, for convenience, we've redefined the difference matrices as $D_1 = D_h, D_2 = D_v, D_3 = D_d, D_4 = D_b$. Since difference matrices are block circulant structures, the multiplication of the matrix can be rewritten as a convolution in two dimensions, that is,

$$D_i u = vec(K_i * U), \quad \mathrm{i} = 1, 2, 3, 4 \tag{12}$$

here $K_1 = [-1, 1], K_2 = [-1, 1]^T, K_3 = \begin{bmatrix} 0 & -1 \\ 1 & 0 \end{bmatrix}$ and $K_4 = \begin{bmatrix} -1 & 0 \\ 0 & 1 \end{bmatrix}$ represent the convolution kernels in the horizontal, vertical, diagonal and back-diagonal direction, respectively. The symbol $*$ is the two dimensional convolution operator.

Obviously, the new model is a typical constrained convex optimization problem, so we use alternating direction multipliers algorithm based on augmented Lagrange method (ADMM) to tackle it. By introducing split variables $x_i = D_i u$ and dual variables $\tilde{x}_i$, (i = 1, 2, 3, 4), equation (11) can be transformed into an unconstrained problem. Its augmented Lagrange objective function can be expressed as:

$$L_A(u, x_i, \tilde{x}_i) = \max_{\tilde{x}_i}\min_{u,x_i} \frac{1}{2}\|f-u\|_2^2 + \mu\sum_{i-1}^{4}\varphi(x_i) + \frac{\beta}{2}\sum_{i=1}^{4}\|x_i - D_i u - \tilde{x}_i\|_2^2 \tag{13}$$

where $\beta > 0$ is the penalty parameter. In this paper, ADMM algorithm is adopted to split the optimization problem into several separate sub-problems, and a saddle point of $L_A(\cdot)$ is obtained by alternatively minimizing the variables $u, x_i, \tilde{x}_i$ under the augmented Lagrangian function $L_A(\cdot)$. The specific solutions are as follows:

$$\begin{aligned} U^{k+1} &= \arg\min_U L_A(U, X_i^k, \tilde{X}_i^k) \\ X_i^{k+1} &= \arg\min_{X_i} L_A(U^{k+1}, X_i, \tilde{X}_i^k) \\ \tilde{X}_i^{k+1} &= \tilde{X}_i^k + \beta(K_i * U^{k+1} - X_i^{k+1}) \end{aligned} \tag{14}$$

Since the variables $(u, x_i, \tilde{x}_i)$ are decoupled in the ADMM framework, so that we investigate these sub-problems one by one. Then the minimization problem with respect to u is as follows:

$$u^{k+1} = \arg\min_u \frac{1}{2}\|f-u\|_2^2 + \frac{\beta}{2}\sum_{i=1}^{4}\left\|x_i^k - D_i u - \tilde{x}_i^k\right\|_2^2 \tag{15}$$

Let the first-order derivative of u as zero, and modify $x_i, \tilde{x}_i$ to get:

$$u - f - \beta\sum_{i=1}^{4} D_i^T(x_i - \tilde{x}_i) + \beta\sum_{i=1}^{4} D_i^T D_i u = 0 \tag{16}$$

Equation (16) can be solved by pseudo inverse or conjugate gradient method, but the computational complexity of multiplication is too high. In order to effectively avoid large matrices multiplication, equation (13) is rewritten in the form of the convolution of matrices, that is:

$$L_A(U, X_i, \tilde{X}_i) = \max_{\tilde{X}_i}\min_{U,X_i} \frac{1}{2}\|F-U\|_2^2 + \mu\sum_{i-1}^{4}\varphi(X_i) + \frac{\beta}{2}\sum_{i=1}^{4}\left\|X_i - K_i * U - \tilde{X}_i\right\|_2^2 \tag{17}$$

where V_i are the matrix form of v_i. We use FFT to transform the time-domain image difference operation into the frequency domain. The frequency domain expression of the U sub-problem is:

$$\bar{U}^{k+1} = \arg\min_{\bar{U}} \frac{1}{2}\left\|\bar{F} - \bar{U}\right\|_2^2 + \frac{\beta}{2}\sum_{i=1}^{4}\left\|\bar{X}_i^k - \bar{K}_i \circ \bar{U} - \bar{\tilde{X}}_i^k\right\|_2^2 \tag{18}$$

where $\bar{V}$ represents the spectrum of V, the symbol $\circ$ represents component-wise multiplication. Obviously, the $\bar{U}$ sub-problem is a least squares problem. By making the first-order derivative of $\bar{U}$ as zero, it is equivalent to the following equation:

$$\bar{U} - \bar{F} + \beta\sum_{i=1}^{4}\bar{K}_i^* \circ \bar{K}_i \circ \bar{U} - \beta\sum_{i=1}^{4}\bar{K}_i \circ (\bar{X}_i - \bar{\tilde{X}}_i) = 0 \tag{19}$$

where $\bar{V}^*$ is the conjugation map of $\bar{V}$. Noted that we use periodic boundary condition here, so $\bar{K}_i^* \circ \bar{K}_i$ is the block circulant with circulating block (BCCB) structure. Hence, the

optimal solution of the Usub-problem can be obtained by using 2D inverse FFT as follows:

$$U^{k+1} = F_{2D}^{-1}\left\{\frac{\bar{F} + \beta\sum_{i=1}^{4}\bar{K}_i \circ (\bar{X}_i - \bar{\tilde{X}}_i)}{1 + \beta\sum_{i=1}^{4}\bar{K}_i^* \circ \bar{K}_i}\right\} \tag{20}$$

The sub-problem of X_i, (i = 1, 2, 3, 4) correspond to the following optimization problem:

$$X_i^{k+1} = \arg\min_{X_i} \mu\varphi(X_i) + \frac{\beta}{2}\left\|X_i - K_i * U^{k+1} - \tilde{X}_i^k\right\|_2^2 \tag{21}$$

The X_i sub-problem belongs to overlapping group and sparse problem, which can be iteratively solved by majorization-minimization (MM) algorithm. More details about MM algorithm can be referred to the literature [32].

Finally, updating the dual variables $\tilde{X}_i$(i = 1, 2, 3, 4)

$$\tilde{X}_i^{k+1} = \tilde{X}_i^k + \beta(K_i * U^{k+1} - X_i^{k+1}) \tag{22}$$

In summary, this paper proposes a new model based on four-directional total variation with overlapping group sparsity (OGSTV4) for image denoising. The specific algorithm is presented as algorithm 2.

Algorithm2: OGSTV4

1: Input U, parameters $\mu > 0$, group size K,

2: Initialize $F_0 = U, k = 0, X_i^0 = 0, \tilde{X}_i^0 = 0$, (i = 1, 2, 3, 4), β

3: Iteration:

$$U^{k+1} = F_{2D}^{-1}\left\{\frac{\bar{H}^* \circ \bar{F} + \beta\sum_{i=1}^{4}\bar{K}_i \circ (\bar{X}_i - \bar{\tilde{X}}_i)}{\bar{H}^* \circ \bar{H} + \beta\sum_{i=1}^{4}\bar{K}_i^* \circ \bar{K}_i}\right\}$$

$$X_i^{k+1} = \arg\min_{X_i} \mu\varphi(X_i) + \frac{\beta}{2}\left\|X_i - K_i * U^{k+1} - \tilde{X}_i^k\right\|_2^2$$

$$\tilde{X}_i^{k+1} = \tilde{X}_i^k + \beta(K_i * U^{k+1} - X_i^{k+1})$$

$$k = k + 1$$

4: If U^{k+1} satisfies the stopping criteria, return U^{k+1} and stop.

A. CONVERGENCE

The new model we proposed is obviously convex. In view of this convexity, the convergence of algorithm 2 can be guaranteed by ADMM theory [35]. It is clear that the ADMM algorithm converges even if each subproblem is not solved exactly. More specifically, the ADMM algorithm converges to the solution of the objective function when the error sequence of subproblems can be summed. Obviously, algorithm 2 is an instance of ADMM. In algorithm 2, the subproblems of $(U, X_i, \tilde{X}_i)$ have closed form solutions. For example, using MM algorithm to solve the subproblem involving X_i is also proved to be convergent in [36].

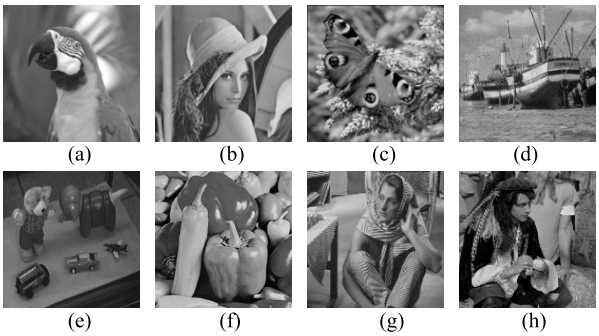

FIGURE 2. Test images.(a) Parrotgray(512*512), (b) Lena(512*512), (c)Butterfly (450*450), (d)Boat(512*512), (e)Toys(256*256), (f)Peppers(256*256),(g)Barbara(512*512), (h)Man(1024*1024).

IV. EXPERIMENTAL RESULTS AND ANALYSIS

To demonstrate the performance of the proposed model for image denoising in this paper, we compare the new model with other state-of-the-art models. The images used in all experiments are shown in Figs.2 with the size of from 256 × 256 to 1024 × 1024. All the experiments were carried out on a system running Windows 10 education version 64-bit with MATLAB version R2015b with an Intel Core i5-2400m CPU at 3.10GHz, with a physical memory of 4GB.

The peak signal to noise ratio (PSNR), structural similarity (SSIM), and computation time (in seconds) are used for the evaluation of the restored image quality. PSNR is defined as:

$$PSNR = 10\log_{10}\frac{Max_{F,\hat{F}}^2}{\left\|F - \hat{F}\right\|_2^2} \tag{23}$$

where F is the original image and $\hat{F}$ is the recovered image. $Max_{F,\hat{F}}^2$ is the maximum possible pixel value of image F and $\hat{F}$. The larger PSNR value, better is the image quality. SSIM is an index to measure the similarity between two images. The specific definition is as follows:

$$\text{SSIM} = \frac{2\mu_F\mu_{\hat{F}}(2\sigma + c_2)}{(\mu_F^2 + \mu_{\hat{F}}^2 + c_1)(\sigma_F^2 + \sigma_{\hat{F}}^2 + c_2)} \tag{24}$$

where μ_F and $\mu_{\hat{F}}$ are the means of F and $\hat{F}$ respectively, σ_F^2 and $\sigma_{\hat{F}}^2$ are the variances of F and $\hat{F}$, σ denotes the covariance, $c_1, c_2 > 0$ are constants. SSIM is less than or equal to 1. The closer SSIM value is to 1, the closer the recovered image is to the original image.

All compared algorithm are set the same stop criterion, that is:

$$\frac{\|U_{k+1} - U_k\|}{\|U_k\|} \le 1 \times 10^{-5} \tag{25}$$

where U_k and U_{k+1} respectively represent the image of the current iteration and the image of the next iteration.

A. PARAMETERS SETTING

Firstly, we adjust the regularization parameter μ, which plays an important role in balancing the data fidelity term and the regularization term. The quality of image restoration largely

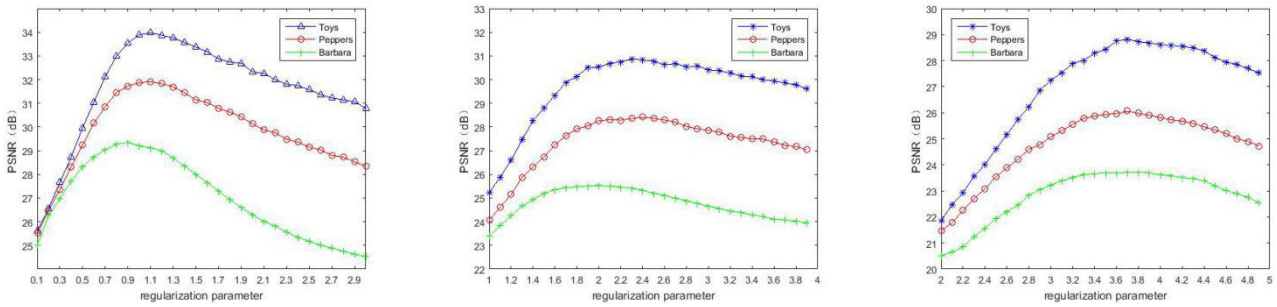

(a) σ=15 (b) σ=30 (c) σ=50

FIGURE 3. PSNR values after image denoising under various values of μ.

depends on the regularization parameter μ. Too lager μ value will cause serious staircase effects. On the contrary, too small μ values will not restore the image well. To illustrate how to choose the suitable parameter μ, we test three images ''Toys'', ''Peppers'' and ''Barbara'' which are degraded by zero-mean Gaussian white noise levels $\sigma = 15$, $\sigma = 30$ and $\sigma = 50$, respectively. We plot the PSNR values after image denoising under various values of regularization parameter μ in Figs. 3. It can be clearly seen that the maximum PSNR values are obtained by different values of μ corresponds to images degraded by different noise levels. When the noise level $\sigma = 15$, we set the range of μ as [0.9,1.2]. When the noise level $\sigma = 30$, the range of μ is selected as [2.0,2.4]. When the noise level $\sigma = 50$, the range of μ is selected as [3.5,3.8].

In order to study the influence of different group size K on the proposed model, we firstly fixed other parameters for the experiment, and then selected images Lena, Parrotgray and Butterfly corrupted by zero-mean Gaussian white noise with a standard deviation of 15 to study the changes of image PSNR and SSIM under different group size. From Figs.4, it is obvious that the maximum PSNR and SSIM are obtained when group size $K = 3$. Therefore, we set the group size to $K = 3$.

Then, the inner iteration numbers N of MM algorithm under the OGS sub-problem are adjusted. We set the iteration numbers N to be 1, 5, 10, 20, 100, 500 and present their effects on PSNR, SSIM and computation time respectively. Here, two pictures of Lena and Peppers are selected to study the choice of N.They are uniformly corrupted by zero-mean Gaussian white noise with standard deviation of 15. From Table 1, we can conclude that the inner iteration numbers do not affect the change of PSNR and SSIM. The computation time is proportional to the inner iteration numbers. Hence, the more iterations, the longer the time. Therefore, the inner iteration numbers are set as $N = 5$.

Theoretically ADMM converges to any positive penalty parameter β. However, choosing the right value of β is crucial for the speed of the algorithm. Since the optimal value of β is different for various experimental pictures, so far there is no method to choose the optimal penalty parameter [37].We set the range of β as [1.0,3.0] empirically.

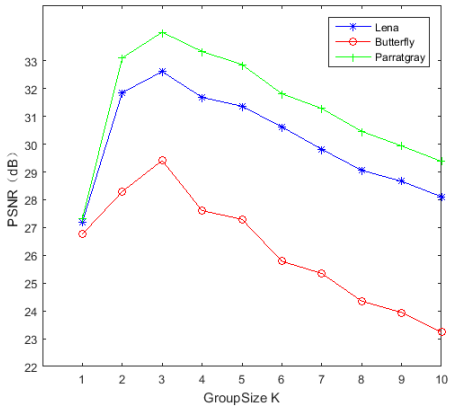

(a)PSNR values under different group sizes

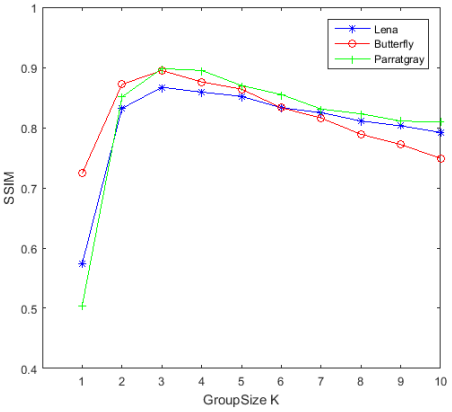

(b) SSIM values under different group sizes

FIGURE 4. PSNR and SSIM values after image denoising under different group sizes.

B. IMAGE DENOSING

In this section, this paper focus on denoising cases of degraded images from Gaussian white noise pollution. Based on the previous discussion, the proposed new model (OGSTV4) was compared with other popular models. Each experimental picture was corrupted by the zero-mean Gaussian white noise with the standard deviation of 15,30 and 50, respectively, and was averaged ten times. Then, PSRN, SSIM and computation time were introduced to evaluate the image quality after denoising.

TABLE 1. Image restoration results for different MM iterations.

σ	Image	inner iteration N	PSNR(dB)	SSIM	Time(s)
15	Lena	1	31.701	0.810	6.474
		5	32.573	0.865	10.219
		10	32.653	0.868	15.235
		20	32.632	0.868	24.063
		100	32.667	0.869	92.119
		500	32.662	0.869	436.031
15	Peppers	1	30.978	0.840	1.273
		5	31.897	0.900	1.593
		10	31.974	0.902	2.071
		20	31.902	0.900	3.064
		100	31.830	0.900	11.337
		500	31.826	0.899	42.227

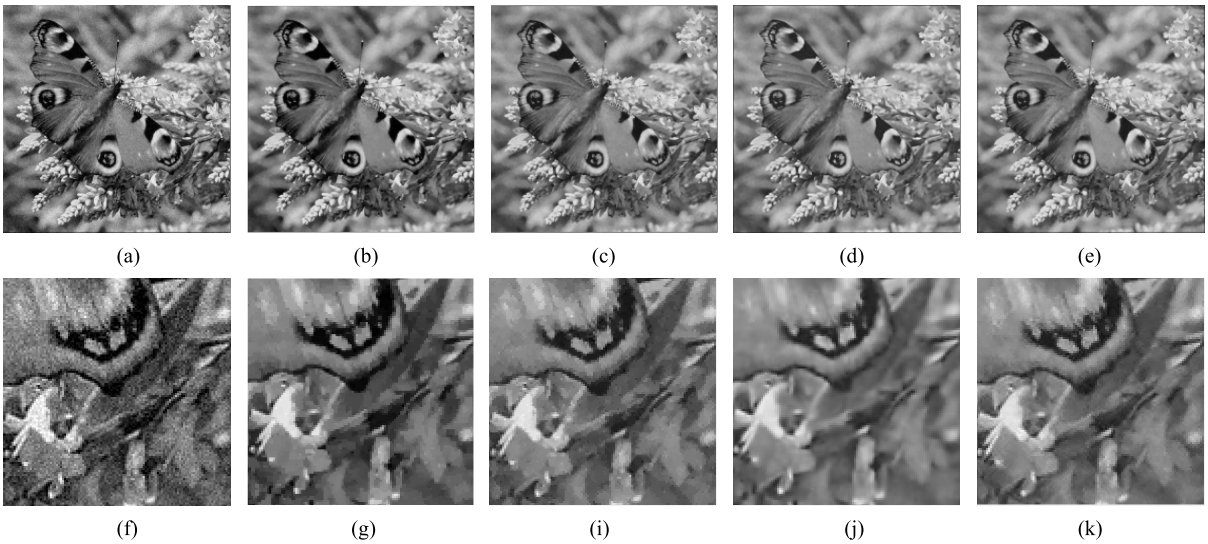

FIGURE 5. Denoised images for Butterfly($\sigma = 15$). (a) Noisy image, (b) TV+BOX restored, (c) TV4 restored, (d) OGSTV restored, (e) OOGSTV4 restored, (f)-(j) zoomed-in images of respective models. In our proposed model, $\mu = 0.9$, $\beta = 1.0$.

1) COMPARISON WITH RELEVANT MODELS

First of all, we demonstrate the superiority of the new model by comparing the relevant models TV+BOX[16], TV4[29] and OGSTV[34]. Here, four images of Parrotgray, Lena, Butterfly and Bridge are selected for the experiment. Adjusting the parameter values for the new model (OGSTV4) aims to find the maximum PSNR and SSIM, which can be seen in section 4.1 for specific parameter values. For OGSTV, we tune the regularization parameter and other parameter values referred to in the literature [18]. TV+BOX and TV4 are also solved by ADMM algorithm, and the best PSNR and SSIM values are obtained by adjusting the parameter values.

Figure 5, 6, and 7 respectively show the overall and local results of restored images by different models for removing Gaussian white noise with standard deviation of 15, 30 and 50. As can be seen from the figure, the TV model adding box constraints and TV4 model can effectively remove noise, it also over smoothes the image edges. Although the OGSTV model have preserved image edge information, but the noise has not been completely eliminated, especially in the corresponding zoomed-in images. The proposed model overcomes the above disadvantages well, not only keeps the good characteristics of traditional TV to eliminate noise, but also fully mines the gradient information of four directions on the image, and then combine them to further suppress staircase effects.

For comparing performance more specifically, Table 2 lists PSNR, SSIM and time (in seconds) values of the restored images by different models. From Table 2, the proposed model always obtain higher values concerning PSNR and SSIM than those of TV+BOX, TV4 and OGSTV. Although

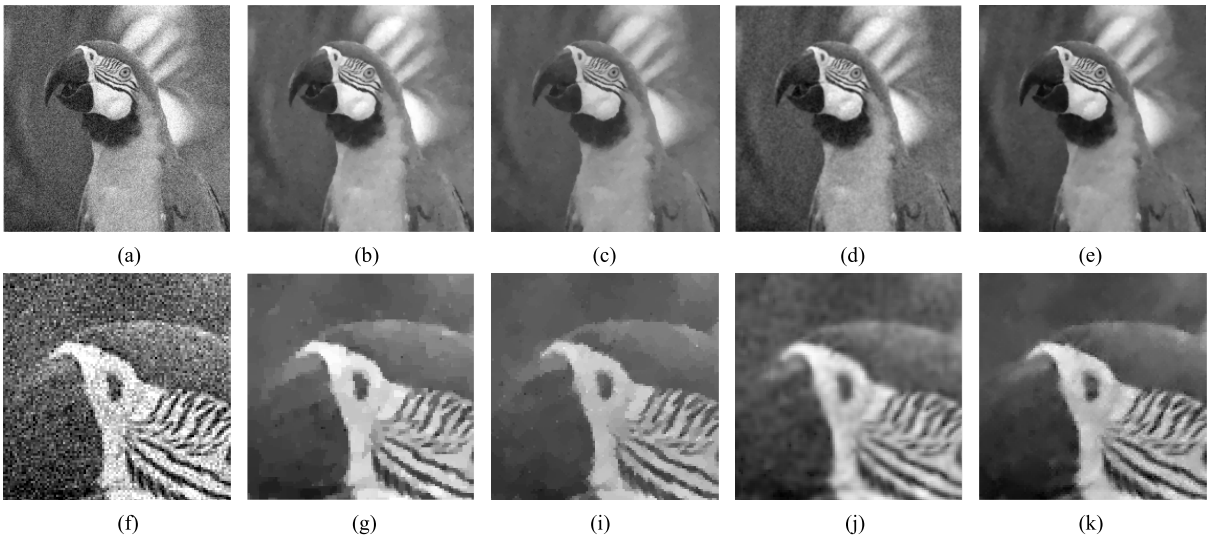

FIGURE 6. Denoised images for Parrotgray($\sigma = 30$). (a) Noisy image, (b) TV+BOX restored, (c) TV4 restored, (d) OGSTV restored, (e) OOGSTV4 restored, (f)-(j) zoomed-in images of respective models. In our proposed model, $\mu = 2.4$, $\beta = 1.0$.

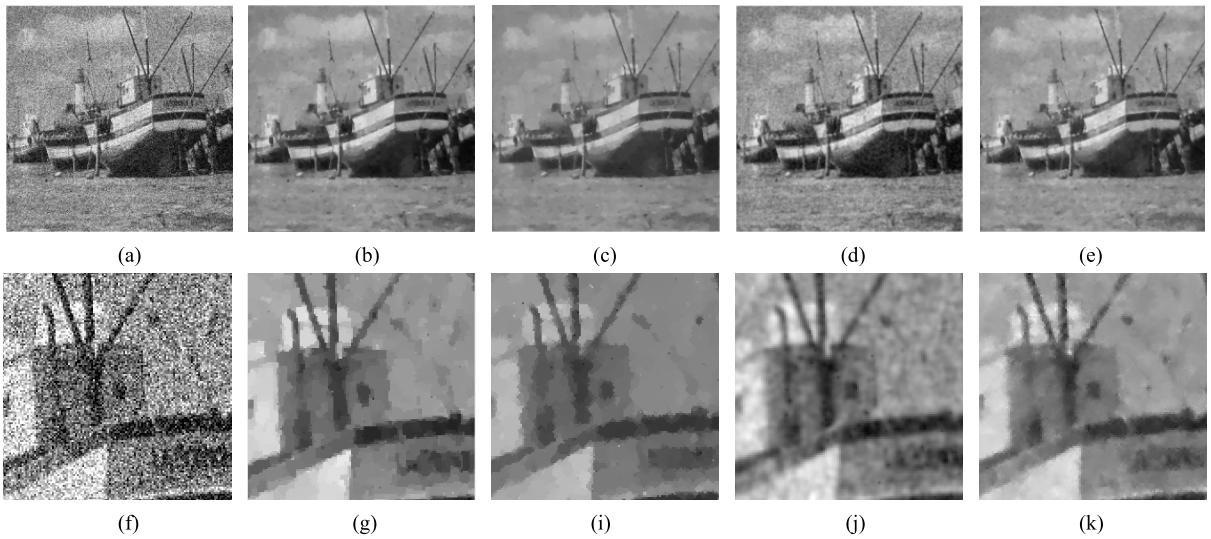

FIGURE 7. Denoised images for Boat($\sigma = 50$). (a) Noisy image, (b) TV+BOX restored, (c) TV4 restored, (d) OGSTV restored, (e) OOGSTV4 restored, (f)-(j) the zoomed-in images of respective models. In our proposed model, $\mu = 3.7$, $\beta = 1.0$.

in terms of time, other models are faster than ours, considering the overall denoising effect, we can conclude that the proposed model is better in denoising.

2) COMPARISON WTH STATE-OF-THE-ART MODELS

To further illustrate the superiority of the proposed model, we compare it with the TGV[10], HDTV[9], and HNHOTV[20] models. Similarly, we test four pictures Toys, Peppers, Barbara and Man. For the TGV model, we set the parameters $\lambda_1 = 2$ and $\lambda_2 = 1$. For the HDTV model, we choose the derivative order as $n = 2$, and then, adjust the regularization parameters of these models to get the maximum PSNR and SSIM values.

In Figures 8, 9 and 10, we represent the denoised images by different models for removing Gaussian white noise with a standard deviation of 15, 30 and 50 respectively. Although the HDTV model can effectively remove the noise, it does not preserve details such as image edges. TGV model alleviate staircase effects while eliminating the noise, but it will produce false image features when the image is highly polluted by noise, which can be seen in Figure 9 (i). Visually, there is no significant difference between the HNHOTV model and the OGSTV4 model. Both of them can achieve a balance preserving edges and noise removal, and reduce staircase artifacts.

The PSNR, SSIM and Time (in seconds) values obtained by different models are presented in Tables 3. As shown in Table 3, our proposed model performs best in most cases. Compared with other models, the proposed model is obviously higher in SSIM value, and basically higher

TABLE 2. PSNR, SSIM and Time values of the restored images denoised by different models.

σ	Image	TV+BOX PSNR(dB)/SSIM/Time(s)	TV4 PSNR(dB)/SSIM/Time(s)	OGSTV PSNR(dB)/SSIM/Time(s)	OGSTV4 PSNR(dB)/SSIM/Time(s)
15	Parrotgray	33.188/0.861/1.336	33.527/0.893/3.264	32.886/0.834/1.109	**33.970/0.894**/5.978
	Lena	31.938/0.839/1.654	31.922/0.851/4.283	32.197/0.833/1.579	**32.633/0.866**/7.790
	Butterfly	29.231/0.877/1.529	29.060/0.871/4.023	28.547/0.889/1.545	**29.483/0.895**/8.327
	Boat	30.493/0.812/1.864	29.917/0.801/4.371	30.626 /0.814/1.734	**30. 720/0.822**/8.822
30	Parrotgray	30.233/0.825/1.324	30.165/0.823/3.172	28.913/0.741/1.072	**30.777/0.857**/4.771
	Lena	29.085/0.779/1.879	28.964/0.785/4.078	28.661/0.753/1.638	**29.588/0.809**/6.191
	Butterfly	25.402/0.777/1.570	25.204/0.772/3.631	24.800/0.770/1.349	**25.793/0.802**/7.222
	Boat	27.395/0.715/1.800	27.093/0.704/4.081	27.116/0.682/1.761	**27.573/0.726**/7.149
50	Parrotgray	28.027/0.806/3.911	28.021/0.794/4.507	26.347/0.719/1.384	**28.402/0.842**/8.059
	Lena	27.123/0.736/5.983	27.040/0.727/6.692	26.464/0.691/2.154	**27.428/0.758**/7.607
	Butterfly	23.173/0.673/4.968	22.943/0.647/4.299	22.895/0.633/1.783	**23.387/0.704**/7.338
	Boat	25.325/0.632/6.307	25.148/0.625/6.060	24.839/0.609/2.118	**25.564/0.645**/8.914

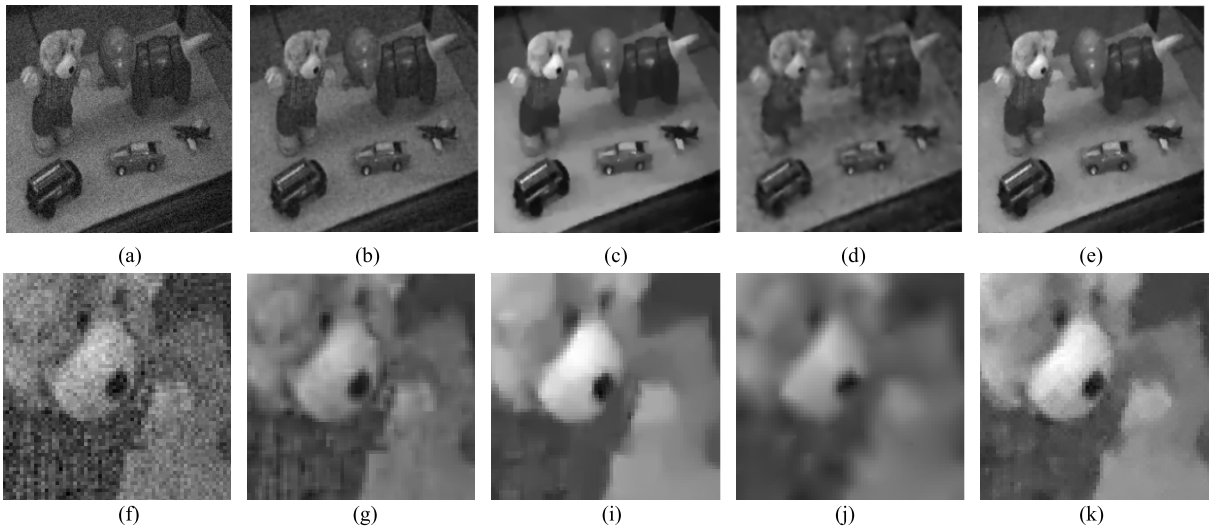

FIGURE 8. Denoised images for Toys($\sigma = 15$). (a) Noisy image, (b) HDTV restored, (c) HNHOTV restored, (d) TGV restored,(e)OOGSTV4 restored, (f)-(j) zoomed-in images of respective models. In our proposed model, $\mu = 1.2$, $\beta = 1.0$.

TABLE 3. PSNR, SSIM and Time values of the restored image denoised by different models.

σ	Image	HDTV PSNR(dB)/SSIM/Time(s)	HNHOTV PSNR(dB)/SSIM/Time(s)	TGV PSNR(dB)/SSIM/Time(s)	OGSTV4 PSNR(dB)/SSIM/Time(s)
15	Toys	33.707/0.851/2.816	33.488/0.897/2.914	33.239/0.803/2.889	**33.948/0.902**/1.708
	Peppers	31.609/0.860/1.790	31.762/0.872/2.518	30.633/0.864/2.921	**31.945/0.907**/1.789
	Barbara	28.875/0.797/6.492	**29.237**/0.846/13.647	28.353/0.801/15.683	29.047/**0.851**/11.428
	Man	31.682/0.809/35.693	31.940/0.854/82.663	31.928/0.796/73.57	**31.998/0.880**/69.935
30	Toys	30.450/0.817/2.832	30.957/0.843/2.881	30.792/0.798/2.869	**30.996/0.847**/1.454
	Peppers	28.013/0.774/1.768	**28.400**/0.846/2.826	28.166/0.829/2.97	28.372/**0.851**/1.492
	Barbara	24.955/0.681/13.633	25.488/0.720/17.781	24.868/0.696/15.732	**25.517/0.737**/11.478
	Man	27.921/0.709/71.574	28.651/0.722/103.545	27.873/0.694/398.39	**28.879/0.785**/91.537
50	Toys	28.318/0.717/5.880	28.716/0.774/3.144	28.417/0.723/2.998	**28.751/0.791**/1.374
	Peppers	25.864/0.727/3.078	25.753/0.743/2.843	26.055/0.762/2.897	**26.065/0.788**/1.335
	Barbara	23.246/0.616/23.104	**23.736**/0.631/16.952	23.447/0.622/5.810	23.694 /**0.648**/8.942
	Man	27.057/0.678/99.837	27.692/0.710/144.394	27.383/0.684 /564.23	**27.834/0.725**/116.669

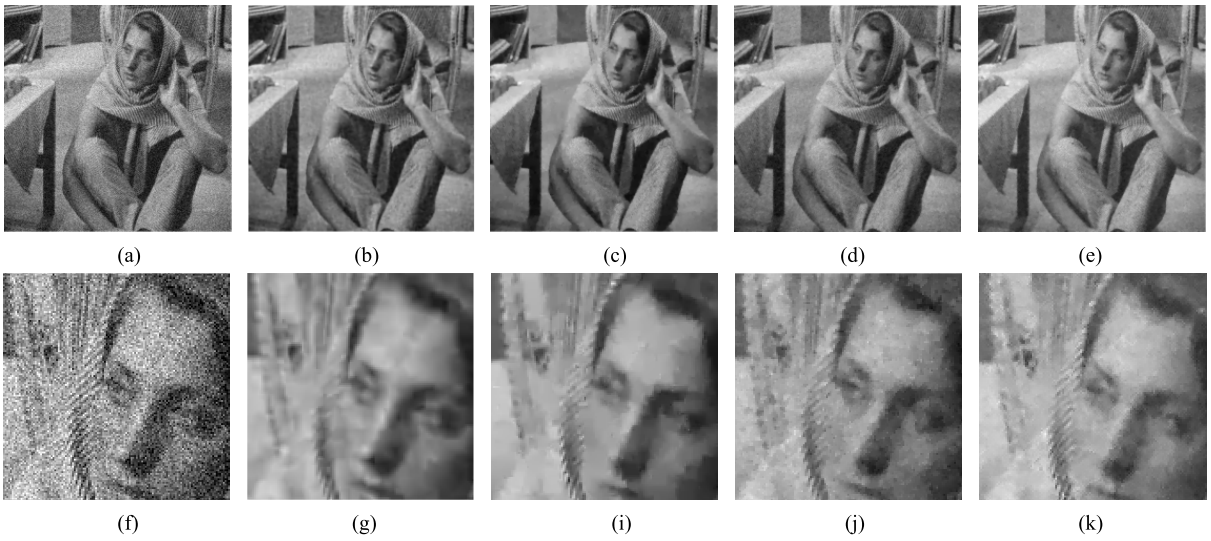

FIGURE 9. Denoised images for Barbara($\sigma = 30$). (a) Noisy image, (b) HDTV restored, (c) HNHOTV restored, (d) TGV restored, (e) OOGSTV4 restored, (f)-(j) zoomed-in images of respective models. In our proposed model, $\mu = 2.0$, $\beta = 1.0$.

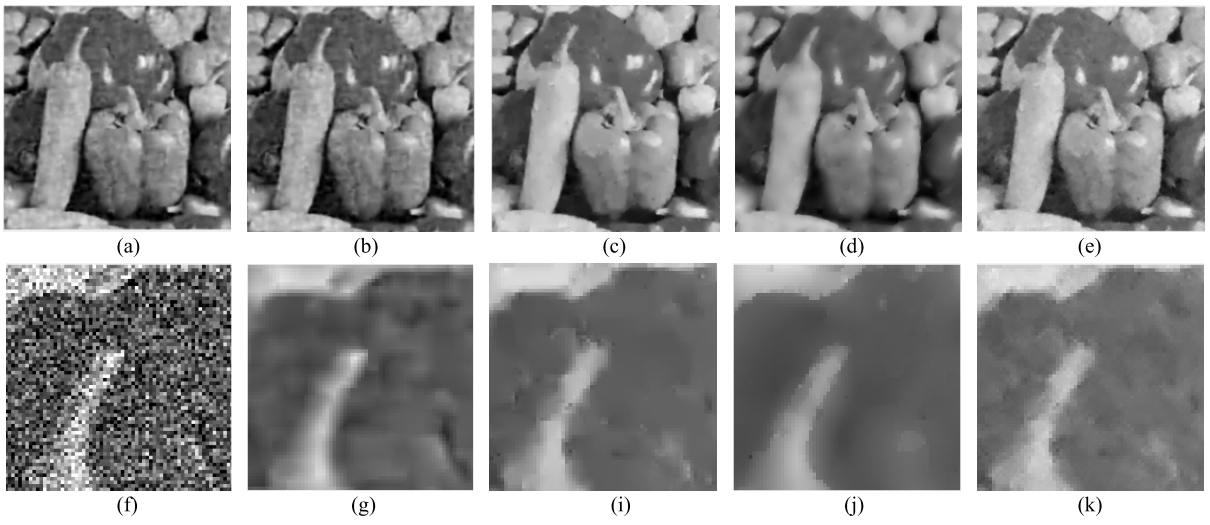

FIGURE 10. Denoised images for Peppers($\sigma = 50$). (a) Noisy image, (b) HDTV restored, (c) HNHOTV restored, (d) TGV restored, (e) OOGSTV4 restored, (f)-(j) the zoomed-in images of respective models. In our proposed model, $\mu = 3.9$, $\beta = 0.8$.

in PSNR value, except for HNHOTV which is higher in image Peppers and Barbara. In terms of time, the computation time of the new model is moderate, which is significantly less than that of HNHOTV. Considering this, our model outperforms other models in denoising.

3) COMPARISON OF THE PROPOSED MODEL WITH BOX CONSTRAINT OR WITHOUT

It should be noted that the pixel value of any digital image can only obtain a finite pixel value (for instance, an 8bit image can only have 256 gray grayscale levels). Therefore, adding box constraints is required to ensure all pixel values of the recovered image within a certain dynamic range, which greatly improves the quality of the recovered image. Motivated by the constrained TV model proposed by Chan [16], we also add box constraints to the proposed new model, which is referred to as the OGSTV4+BOX model.

Then, two pictures Peppers and Lean are used for this experiment, which are corrupted by zero-mean Gaussian white noise with standard deviation $\sigma = 15$. We compare the proposed model with the OGSTV4+BOX model. The denoising results can be seen in Figs.11. There is no specific difference between the proposed model and one after adding box constraint. From PSNR, it is indeed higher than the proposed model without box constraint, but the time also increases accordingly. Hence, we still choose the proposed model after comprehensive consideration.

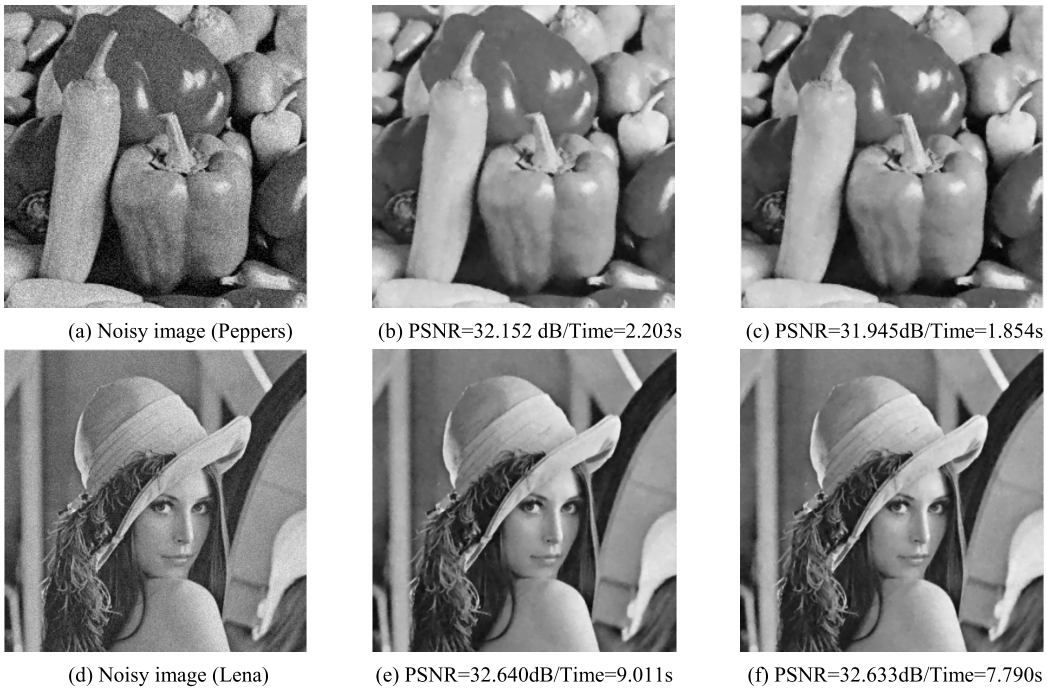

(a) Noisy image (Peppers) (b) PSNR=32.152 dB/Time=2.203s (c) PSNR=31.945dB/Time=1.854s

(d) Noisy image (Lena) (e) PSNR=32.640dB/Time=9.011s (f) PSNR=32.633dB/Time=7.790s

FIGURE 11. Denoised images ($\sigma = 15$). (a),(d) Noisy image, (b), (e) OGSTV4+BOX restored, (c), (f) OGSTV4 restored.

V. CONCLUSION

In this paper, an effective image denoising model is proposed by using four-directional total variation and overlapping group sparsity. We divide the complex optimization problem into several independent subproblems by introducing split and dual variables into ADMM algorithm, and then, solve the corresponding subproblems alternatively by using FFT and MM algorithm. To illustrate the superiority of our new model, we compare our model with other state-of-the-art models and introduce PSNR, SSIM and computation time to evaluate the image quality after denoising. The proposed model removes noise effectively and preserves image feature well to get better image quality. Meanwhile, the staircase effects can be suppressed successfully. However, we can see that although the new model is very robust in denoising, the denoising time is relatively long. We will consider how to improve this in our next work.

REFERENCES

[1] A. N. Tikhonov and V. Y. Arsenin, "Solutions of ill-posed problems," *Math. Comput.*, vol. 32, no. 144, p. 491, Apr. 1979.

[2] K. He, X. Zhang, S. Ren, and J. Sun, "Deep residual learning for image recognition," in *Proc. IEEE Conf. Comput. Vis. Pattern Recognit. (CVPR)*, Las Vegas, NV, USA, Jun. 2016, pp. 770–778, doi: 10.1109/CVPR.2016.90.

[3] K. Zhang, W. Zuo, Y. Chen, D. Meng, and L. Zhang, "Beyond a Gaussian denoiser: Residual learning of deep CNN for image denoising," *IEEE Trans. Image Process.*, vol. 26, no. 7, pp. 3142–3155, Jul. 2017, doi: 10.1109/TIP.2017.2662206.

[4] K. Zhang, W. Zuo, and L. Zhang, "FFDNet: Toward a fast and flexible solution for CNN-based image denoising," *IEEE Trans. Image Process.*, vol. 27, no. 9, pp. 4608–4622, Sep. 2018, doi: 10.1109/TIP.2018.2839891.

[5] M. Lysaker and X.-C. Tai, "Iterative image restoration combining total variation minimization and a second-order functional," *Int. J. Comput. Vis.*, vol. 66, no. 1, pp. 5–18, Jan. 2006.

[6] Z. Xian-Chun, W. Mei-Ling, Z. Lin-Feng, and W. Qin, "Image denoising model based on the improved demons algorithm," *Acta Phys. Sinica*, vol. 64, no. 2, 2015, Art. no. 024205, doi: 10.7498/aps.64.024205.

[7] K. Dabov, A. Foi, V. Katkovnik, and K. Egiazarian, "Image denoising by sparse 3-D transform-domain collaborative filtering," *IEEE Trans. Image Process.*, vol. 16, no. 8, pp. 2080–2095, Aug. 2007, doi: 10.1109/TIP.2007.901238.

[8] L. I. Rudin, S. Osher, and E. Fatemi, "Nonlinear total variation based noise removal algorithms," *Phys. D, Nonlinear Phenomena*, vol. 60, nos. 1–4, pp. 259–268, Nov. 1992.

[9] Y. Hu, G. Ongie, S. Ramani, and M. Jacob, "Generalized higher degree total variation (HDTV) regularization," *IEEE Trans. Image Process.*, vol. 23, no. 6, pp. 2423–2435, Jun. 2014, doi: 10.1109/TIP.2014.2315156.

[10] K. Bredies, K. Kunisch, and T. Pock, "Total generalized variation," *SIAM J. Imag. Sci.*, vol. 3, no. 3, pp. 492–526, 2010.

[11] R. W. Liu, L. Shi, W. Huang, J. Xu, S. C. H. Yu, and D. Wang, "Generalized total variation-based MRI rician denoising model with spatially adaptive regularization parameters," *Magn. Reson. Imag.*, vol. 32, no. 6, pp. 702–720, Jul. 2014.

[12] X. Xu, T. Yu, X. Xu, G. Hou, R. W. Liu, and H. Pan, "Variational total curvature model for multiplicative noise removal," *IET Comput. Vis.*, vol. 12, no. 4, pp. 542–552, Jun. 2018, doi: 10.1049/iet-cvi.2017.0332.

[13] G. Gilboa and S. Osher, "Nonlocal operators with applications to image processing," *Multiscale Model. Simul.*, vol. 7, no. 3, pp. 1005–1028, 2008.

[14] R. W. Liu, L. Shi, S. C. H. Yu, and D. Wang, "A two-step optimization approach for nonlocal total variation-based rician noise reduction in magnetic resonance images," *Med. Phys.*, vol. 42, no. 9, pp. 5167–5187, Aug. 2015.

[15] J.-H. Yang, X.-L. Zhao, J.-J. Mei, S. Wang, T.-H. Ma, and T.-Z. Huang, "Total variation and high-order total variation adaptive model for restoring blurred images with cauchy noise," *Comput. Math. with Appl.*, vol. 77, no. 5, pp. 1255–1272, Mar. 2019.

[16] R. H. Chan and J. Ma, "A multiplicative iterative algorithm for box-constrained penalized likelihood image restoration," *IEEE Trans. Image Process.*, vol. 21, no. 7, pp. 3168–3181, Jul. 2012, doi: 10.1109/TIP.2012.2188811.

[17] H. Chen, C. Wang, Y. Song, and Z. Li, "Split bregmanized anisotropic total variation model for image deblurring," *J. Vis. Commun. Image Represent.*, vol. 31, pp. 282–293, Aug. 2015.

[18] J. Liu, T.-Z. Huang, I. W. Selesnick, X.-G. Lv, and P.-Y. Chen, "Image restoration using total variation with overlapping group sparsity," *Inf. Sci.*, vol. 295, pp. 232–246, Feb. 2015.
[19] M. Shi, T. Han, and S. Liu, "Total variation image restoration using hyper-Laplacian prior with overlapping group sparsity," *Signal Process.*, vol. 126, pp. 65–76, Sep. 2016.
[20] T. Adam and R. Paramesran, "Image denoising using combined higher order non-convex total variation with overlapping group sparsity," *Multidimensional Syst. Signal Process.*, vol. 30, no. 1, pp. 503–527, Jan. 2019.
[21] A. Kumar, M. O. Ahmad, and M. N. S. Swamy, "A framework for image denoising using first and second order fractional overlapping group sparsity (HF-OLGS) regularizer," *IEEE Access*, vol. 7, pp. 26200–26217, 2019, doi: 10.1109/ACCESS.2019.2901691.
[22] M.-J. Fan and X.-C. Zhou, "High order total variation with overlapping group sparsity for image restoration," (in Chinese), *Appl. Res. Comput.*, vol. 37, no. 10, 2020, Art. no. e0122562.
[23] M. Ding, T.-Z. Huang, S. Wang, J.-J. Mei, and X.-L. Zhao, "Total variation with overlapping group sparsity for deblurring images under cauchy noise," *Appl. Math. Comput.*, vol. 341, pp. 128–147, Jan. 2019.
[24] X.-G. Lv, L. Jiang, and J. Liu, "Deblurring Poisson noisy images by total variation with overlapping group sparsity," *Appl. Math. Comput.*, vol. 289, pp. 132–148, Oct. 2016.
[25] J. Liu, T.-Z. Huang, G. Liu, S. Wang, and X.-G. Lv, "Total variation with overlapping group sparsity for speckle noise reduction," *Neurocomputing*, vol. 216, pp. 502–513, Dec. 2016.
[26] M. Sakurai, S. Kiriyama, T. Goto, and S. Hirano, "Fast algorithm for total variation minimization," in *Proc. 18th IEEE Int. Conf. Image Process.*, Sep. 2011, pp. 1461–1464, doi: 10.1109/ICIP.2011.6115718.
[27] F. Liao, J. L. Coatrieux, J. Wu, and H. Shu, "A new fast algorithm for constrained four-directional total variation image denoising problem," *Math. Problems Eng.*, vol. 2015, pp. 1–11, Jan. 2015.
[28] L. Wu, Y. Chen, J. Jin, H. Du, and B. Qiu, "Four-directional fractional-order total variation regularization for image denoising," *J. Electron. Imag.*, vol. 26, no. 5, p. 1, Sep. 2017, doi: 10.1117/1.JEI.26.5.053003.
[29] Z. Cheng, Y. Chen, L. Wang, F. Lin, H. Wang, and Y. Chen, "Four-directional total variation denoising using fast Fourier transform and ADMM," in *Proc. IEEE 3rd Int. Conf. Image, Vis. Comput. (ICIVC)*, Jun. 2018, pp. 379–383.
[30] M. Tao and J. Yang, "Alternating direction algorithms for total variation deconvolution in image reconstruction," Dept. Mathematics, Rice University, Houston, TX, USA, Res. Rep. TR0918, 2009.
[31] S. Boyd, "Distributed optimization and statistical learning via the alternating direction method of multipliers," *Found. Trends Mach. Learn.*, vol. 3, no. 1, pp. 1–122, 2010.
[32] M. A. T. Figueiredo, J. M. Bioucas-Dias, and R. D. Nowak, "Majorization–minimization algorithms for wavelet-based image restoration," *IEEE Trans. Image Process.*, vol. 16, no. 12, pp. 2980–2991, Dec. 2007.
[33] D. R. Hunter and K. Lange, "A tutorial on MM algorithms," *Amer. Statistician*, vol. 58, no. 1, pp. 30–37, Feb. 2004.
[34] I. W. Selesnick and P.-Y. Chen, "Total variation denoising with overlapping group sparsity," in *Proc. IEEE Int. Conf. Acoust., Speech Signal Process.*, Vancouver, BC, Canada, May 2013, pp. 5696–5700, doi: 10.1109/ICASSP.2013.6638755.
[35] W. Deng and W. Yin, "On the global and linear convergence of the generalized alternating direction method of multipliers," *J. Sci. Comput.*, vol. 66, no. 3, pp. 889–916, Mar. 2016.
[36] B. He and H. Yang, "Some convergence properties of a method of multipliers for linearly constrained monotone variational inequalities," *Oper. Res. Lett.*, vol. 23, nos. 3–5, pp. 151–161, Oct. 1998.
[37] M. A. T. Figueiredo and J. M. Bioucas-Dias, "Restoration of Poissonian images using alternating direction optimization," *IEEE Trans. Image Process.*, vol. 19, no. 12, pp. 3133–3145, Dec. 2010.

XIANCHUN ZHOU was born in Anhui, China, in 1974. He received the B.Sc. degree from Anhui University, in 1998, the M.Sc. degree from the Nanjing University of Posts and Telecommunications, in 2005, and the Ph.D. degree from the Nanjing University of Information Science and Technology, in 2011.

In 2011, he was a Postgraduate Supervisor and an Associate Professor. He was appointed as a Professor with the Nanjing University of Information Science and Technology. He is currently the Dean of the Nanjing University of Information Engineering, and also the Deputy General Manager of the Nanjing Longyuan Technology Center. He has taken charge of and accomplished over ten projects supported by the National Natural Science Foundation, and so on. He has published over 50 journal articles and five books, and has over ten invention patents authorized. His research interests include digital image processing and pattern recognition. He is also the Senior Member of the Chinese Electronic Society and a member of the Chinese Academy of Technology.

MENGJIA FAN was born in Suzhou, Jiangsu, China, in 1996. She received the bachelor's degree in engineering from the Nanjing University of Information Science and Technology, in 2018, where she is currently pursuing the master's degree in electronics and information engineering. Her research interests include digital image processing and computer vision.